

Extensions, Validation, and Clinical Applications of a Feedback Control System Simulator of the Hypothalamo-Pituitary-Thyroid Axis

Marisa Eisenberg,¹ Mary Samuels,² and Joseph J. DiStefano III¹

Background: We upgraded our recent feedback control system (FBCS) simulation model of human thyroid hormone (TH) regulation to include explicit representation of hypothalamic and pituitary dynamics, and updated TH distribution and elimination (D&E) parameters. This new model greatly expands the range of clinical and basic science scenarios explorable by computer simulation.

Methods: We quantified the model from pharmacokinetic (PK) and physiological human data and validated it comparatively against several independent clinical data sets. We then explored three contemporary clinical issues with the new model: combined triiodothyronine (T₃)/thyroxine (T₄) versus T₄-only treatment, parenteral levothyroxine (L-T₄) administration, and central hypothyroidism.

Results: Combined T₃/T₄ therapy—In thyroidectomized patients, the L-T₄-only replacement doses needed to normalize plasma T₃ or average tissue T₃ were 145 μ g L-T₄/day or 165 μ g L-T₄/day, respectively. The combined T₄ + T₃ dosing needed to normalize both plasma and tissue T₃ levels was 105 μ g L-T₄ + 9 μ g T₃ per day. For all three regimens, simulated mean steady-state plasma thyroid-stimulating hormone (TSH), T₃, and T₄ was within normal ranges (TSH: 0.5–5 mU/L; T₄: 5–12 μ g/dL; T₃: 0.8–1.9 ng/mL). Parenteral T₄ administration—800 μ g weekly or 400 μ g twice weekly normalized average tissue T₃ levels both for subcutaneous (SC) and intramuscular (IM) routes of administration. TSH, T₃, and T₄ levels were maintained within normal ranges for all four of these dosing schemes (1 \times vs. 2 \times weekly, SC vs. IM). Central hypothyroidism—We simulated steady-state plasma T₃, T₄, and TSH concentrations in response to varying degrees of central hypothyroidism, reducing TSH secretion from 50% down to 0.1% of normal. Surprisingly, TSH, T₃, and T₄ plasma concentrations remained within normal ranges for TSH secretion as low as 25% of normal.

Conclusions: Combined T₃/T₄ treatment—Simulated standard L-T₄-only therapy was sufficient to renormalize average tissue T₃ levels and maintain normal TSH, T₃, and T₄ plasma levels, supporting adequacy of standard L-T₄-only treatment. Parenteral T₄ administration—TSH, T₃, and T₄ levels were maintained within normal ranges for all four of these dosing schemes (1 \times vs. 2 \times weekly, SC vs. IM), supporting these therapeutic alternatives for patients with compromised L-T₄ gut absorption. Central hypothyroidism—These results highlight how highly nonlinear feedback in the hypothalamic-pituitary-thyroid axis acts to maintain normal hormone levels, even with severely reduced TSH secretion.

Introduction

OUR RECENTLY PUBLISHED FEEDBACK CONTROL system (FBCS) simulation model of human thyroid hormone regulation (1), shown here in Figure 1, had limited predictive capabilities, because it did not explicitly include the dynamics of brain components. We simulated the closed-loop system in that work by replacing the thyroid stimulating hormone (TSH)- and thyrotropin-releasing hormone (TRH)-related submodels—the portions of Figure 1 in the dashed box

marked “Brain Submodels”—with human TSH time-course data, and developed a quantified model of the remaining thyroid hormone (TH) submodels. We used this fixed TSH data, which characterizes the output of this group of subsystem components, together with levothyroxine (L-T₄) oral doses, as dual inputs in the earlier model, and quantified it completely from human clinical data. This permitted simulation of time-varying free and bound triiodothyronine (T₃(t)) and T₄(t)—but not TSH(t) levels in plasma and tissues. We did assess several bioequivalence and replacement hormone

¹Biocybernetics Laboratory, Departments of Computer Science, Medicine, and Biomedical Engineering, UCLA, Los Angeles, California.

²Division of Endocrinology, Diabetes, and Clinical Nutrition, Oregon Health and Sciences Center University, Portland, Oregon.

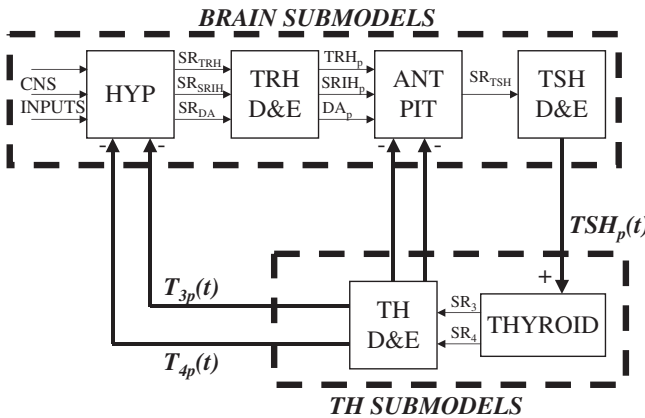


FIG. 1. Overall feedback control system model of thyroid hormone regulation, with three source organ blocks—the hypothalamus (HYP), anterior pituitary (ANT PIT), and thyroid glands (THYROID)—and three sink blocks—for TRH, TSH, and T_3 and T_4 distribution and elimination (elimination = metabolism and excretion) (D&E). TRH, thyrotropin-releasing hormone; TSH, thyroid-stimulating hormone; T_3 , triiodothyronine; T_4 , thyroxine; SR, secretion rate; p, plasma or portal plasma for TRH-related components; DA, dopamine; SRIH, somatostatin.

questions using this model, but further application scenarios were limited to cases where complete time-course TSH(t) data are available for conditions of interest, or when the feedback loop is open, for example, as in thyroidectomized individuals—in which case TSH is inoperative. Explicit models for all six blocks in Figure 1 are needed to more fully address clinical and basic science questions *in silico*, that is, by computer simulation.

We develop, quantify, and validate a quasi-mechanistic representation of the four remaining brain submodel blocks in Figure 1 here, using human closed-loop data for quantifica-

tion and validation of a simplified aggregate of hypothalamus and pituitary components combined, schematized in Figure 2. This new brain submodel is incorporated into the whole FBCS model of the hypothalamic-pituitary-thyroid (H-P-T) axis, thereby rendering it capable of simulating a wider variety of clinical and experimental scenarios, because it characterizes the secretion and distribution and elimination (D&E) (metabolism + excretion) dynamics of all three FBCS variables—TSH(t) as well as $T_3(t)$ and $T_4(t)$, in plasma and tissue pools. We independently validate the new model by comparing it to a variety of other clinical data, reassess predictions made with the earlier model, and also apply it to two additional problems of current clinical interest—regulated responses of all three hormones to parenteral L- T_4 administration and central hypothyroidism.

Methods I: Model Development, Quantification, and Validation

Brain submodels

Lumped hypothalamo-pituitary TSH secretion submodel. Plasma TSH is the primary clinical measure of thyroid function, and therefore must be depicted as a controllable variable, rather than as fixed data, because the primary goal of our extended model is to predict TSH responses to other model/system variables affecting it, such as TH. To accomplish this, we need to adequately describe TSH secretion and D&E dynamics in the closed-loop system, over physiological and pathophysiological ranges, in response to T_3 , T_4 , and other inputs depicted in Figure 1.

Hypothalamic TRH drives pituitary TSH secretion. Unfortunately, sufficient details on hypothalamic component dynamics are unattainable at present, because we lack the data to distinguish it from the pituitary. For example, time-course pituitary portal plasma TRH concentration data, reflecting endogenous TRH secreted by the hypothalamus under physiological conditions, are not measurable, motivating our aggregation approach. Available data can provide a simplified submodel that captures overall pituitary TSH dynamics and the signals that control TSH secretion.

We combined the TRH secretion, TRH D&E, and TSH secretion submodel blocks of Figure 1 into the single, lumped submodel illustrated within the dashed-line box in Figure 2, with a single-output, TSH secretion rate, driven implicitly by TRH, and dual suppressor inputs—plasma T_3 and T_4 concentrations, $T_{3p}(t)$ and $T_{4p}(t)$. TSH secretion is represented as a harmonic oscillator damped by T_3 signals in pituitary and other unspecified brain regions. In this quasi-mechanistic input-output model representation, the identity and pathways for all such T_3 signals are unknown, so we define a single, lumped variable representing equivalent T_3 in relevant portions of the brain, that is, anterior pituitary, hypothalamus, and so on, which affect TSH secretion, directly and via intermediate pathways. We designate this “brain T_3 ” as $T_{3B}(t)$, with its time dependence shown explicitly.

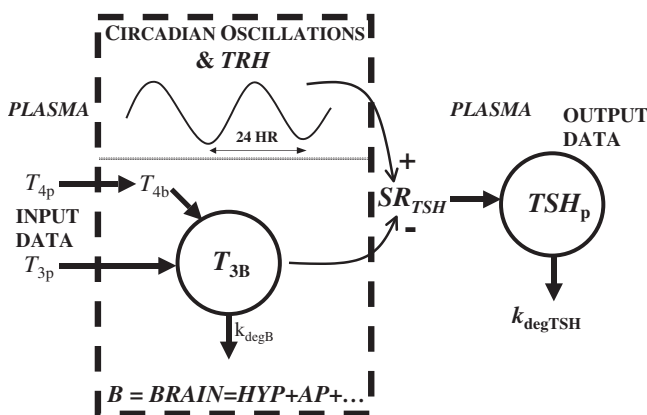


FIG. 2. Simplified brain submodel, structured and quantified from plasma thyroid-stimulating hormone (TSH), triiodothyronine (T_3), and thyroxine (T_4) concentration data. TSH secretion and distribution and elimination are explicit, thyrotropin-releasing hormone (TRH) is implicit, plasma T_3 and T_4 are inputs, and plasma TSH $_p$ is the model output. A new variable: equivalent T_3 in brain, denoted T_{3B} , represents T_3 directly or indirectly affecting TSH secretion and located anywhere in brain.

$$SR_{TSH}(t) = \left(B_0 + A_0 \sin\left(\frac{2\pi}{24}t - \phi_{\text{phase}}\right) \right) e^{-T_{3B}(t)k_{\text{degTSH}}} \quad (1)$$

In this equation, $SR_{TSH}(t)$ is the total TSH secretion rate, and B_0 is the basal TSH secretion rate with no TH. The second term on the right is the circadian TSH secretion rate component, all

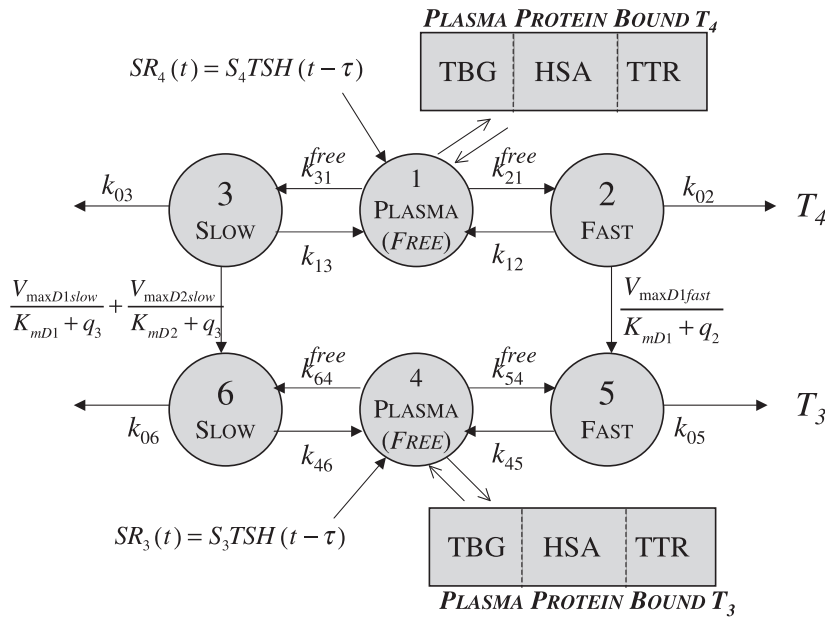


FIG. 3. Nonlinear thyroid hormone distribution and elimination submodel for triiodothyronine (T_3) and thyroxine (T_4) secretion, binding, distribution, interconversion, and elimination in the human. Protein binding submodels are given by $FT_4 = (A + BT_4 + CT_4^2 + DT_4^3)T_{4p}$ and $FT_3 = (a + bT_4 + cT_4^2 + dT_4^3)T_{3p}$ [see Ref. (1) for details]. TBG, T_4 -binding globulin; HSA, human serum albumin; TTR, transthyretin.

damped by brain T_3 , represented as the negative exponent, $T_{3B}(t)$, in the nonlinear exponential term. $2\pi/24$ is the circadian frequency (period 24 hours), ϕ_{phase} is the TSH secretion circadian phase [such that maximum TSH occurs at ~ 2 AM (2)], and A_0 governs the magnitude of circadian oscillations. Effects of TRH are represented implicitly in the sinusoidal daily circadian rhythm and the basal TSH secretion levels.^a

A second equation depicts the dynamics of the unmeasurable and equivalent $T_{3B}(t)$, written in terms of normalized measurable plasma TH levels that presumably regulate $T_{3B}(t)$. We normalized peripheral plasma TH levels, $T_{4p}(t)$ and $T_{3p}(t)$ —to compensate for the roughly 50-fold difference in their plasma concentrations—by dividing them by predose steady-state peripheral plasma levels T_{4pss} and T_{3pss} , which helps in quantifying this submodel.

$$\dot{T}_{3B}(t) = \frac{k_4}{T_{4pss}} T_{4p}(t) + \frac{k_3}{T_{3pss}} T_{3p}(t) - k_{degT3B} T_{3B}(t) \quad (2)$$

The first term of Eq. 2 represents the combined effects of peripheral plasma T_4 (i.e., T_{4p}) on T_{3B} appearance in brain, aggregating peripheral plasma T_4 influx with its intracellular conversion to brain T_3 , $T_{3B}(t)$, at combined fractional rate k_4 (t^{-1}). The second term similarly represents the influx of peripheral plasma T_3 (i.e., T_{3p}) into brain, at effective fractional rate k_3 (t^{-1}). In the third term, k_{degT3B} is the fractional rate of degradation of $T_{3B}(t)$.

TSH D&E submodel A simple one-compartment model adequately describes TSH D&E, with a PCR of 46.1 mL/

min (half-life of 55 minutes) and a distribution volume of 3.5 L (3–5).

TH D&E submodel update Primary components of our earlier simulation model (1) included submodels for T_3 and T_4 secretion (which remain the same in the new model) and for TH D&E, illustrated together in Figure 3. The D&E submodel included TH D&E (metabolism and excretion) in and from plasma, fast and slow tissue pools—including nonlinear T_4 to T_3 conversion and plasma protein binding processes, all as detailed in the equations and compartmental relationships in Figure 3. In the TH D&E submodel, we used *in vitro*-derived K_m values (6) for the deiodinase reactions, because physiological K_m values are unknown. We revisit this submodel here, to explore effects of alternative K_m values reported as being more physiological (6–8), for T_4 deiodination by type I deiodinase (D1). We also check our assumptions about T_4 deiodination by type II deiodinase (D2).

For practical reasons, K_m values are estimated from *in vitro* enzymatic studies, most often performed with dithiothreitol (DTT) as cofactor for the reaction, at concentrations (~ 20 mM) in excess of what is likely to exist *in vivo* for the equivalent and unknown *in vivo* cofactor (7). *In vitro*-derived K_m values for D1 with T_4 have been reported in the $2 \mu\text{M}$ range (6), based on use of ~ 20 mM DTT. DTT does work in assays with reverse T_3 (rT_3) as substrate for D1 at much lower concentrations (0.5 mM) but not with T_4 (7). In contrast, Goswami and Rosenberg (8) used 5 mM glutathione, believed to be a much more physiological cofactor, and estimated the K_m for D1 with T_4 to be 100 times smaller, that is, $K_{mD1}(T_4) \approx 20$ nM. This is the same fold difference found by Sharifi and St. Germain (7) in comparing K_m estimates for D1 with rT_3 at 20 mM versus no added cofactor, suggesting that $K_{mD1}(T_4) \approx 20$ nM, rather than 2 mM, is a better estimate for physiological applications.

In the present work, we updated the value of K_m for D1 with T_4 , now 20 nM instead of $1.9 \mu\text{M}$, based on the above arguments. To check our earlier results with the updated K_m value, we optimally reestimated all TH SR and D&E sub-

^aWe ignore ultradian, 1–2 hours pulsatile TSH oscillations, assuming their small magnitude does not significantly affect downstream TH signals in our model. Additionally, ultradian, unlike circadian rhythms, are not in phase from individual to individual. Our primary database consists of hormone dynamics for the population average. Individual ultradian rhythms are “smoothed out,” with only circadian rhythms prominent in mean data.

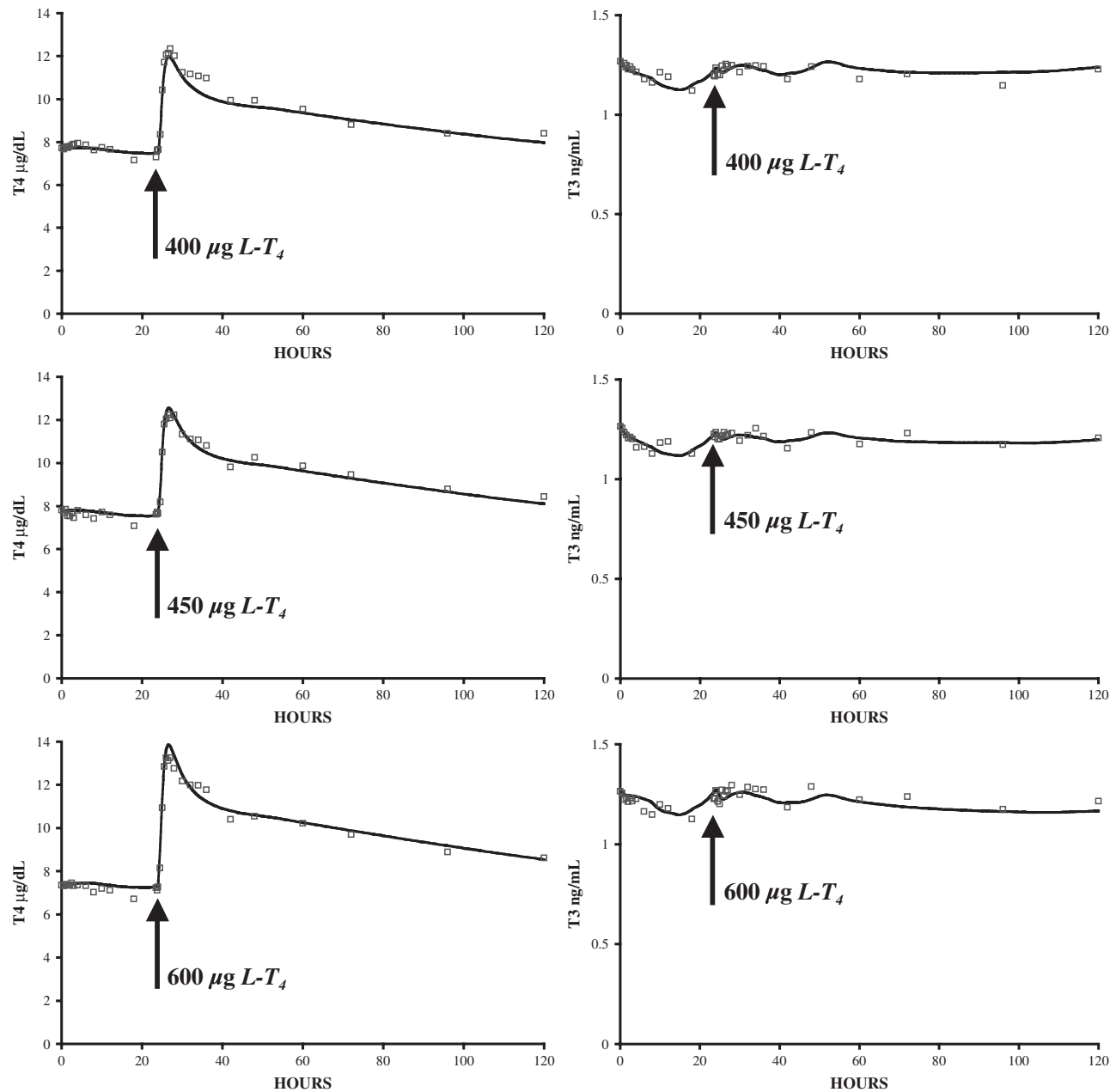


FIG. 4. Updated thyroid submodel fitted to pharmacokinetic data ($n = 33$) (10). Model simulations are shown as solid line and data as squares; thyroxine (T_4) on the left, triiodothyronine (T_3) on the right.

model parameters, using the same kinetic database as before, but with $K_{mD1}(T_4) \approx 20$ nM, and reevaluated our predictive results based on this updated model. Results are given below.

Unfortunately, D2 (and D3) only works *in vitro* with DTT, and there are no data using glutathione as cofactor for the other deiodinases. Although we have no better estimate at this time for the D2 K_m with T_4 as substrate [i.e., 1.5 nM (9)], we did test the sensitivity of our earlier results to this K_m estimate, by optimally refitting the model to ± 10 -fold and ± 100 -fold changes in K_m values used for D2 with T_4 . Results are given below.

Data and model quantification

Primary data Our primary closed-loop database consists of 33 sets of PK data, collected simultaneously for $hTSH_p(t)$,

$T_{3p}(t)$, and $T_{4p}(t)$, over 120 hours in euthyroid volunteers (half male, half female), beginning with baseline levels the day prior to dosing (day -1), in response to three different oral doses of $L-T_4$, 400, 450, and 600 μg , on day 0 (10). Subjects were fasted from 10 PM on day 2 to noon on day -1 and also from 10 PM on day -1 to noon on day 0, putting them in the fasting state until 4 hours after dosing. The data shown averaged in Figures 4 and 5 were generously supplied by the authors (10).

Brain submodel quantification Previously, we used the three plasma TSH data sets (circles in Fig. 5) as input forcing functions and quantified the thyroid and TH D&E submodel from T_3 and T_4 plasma data (Fig. 6, top left) (1). For the new

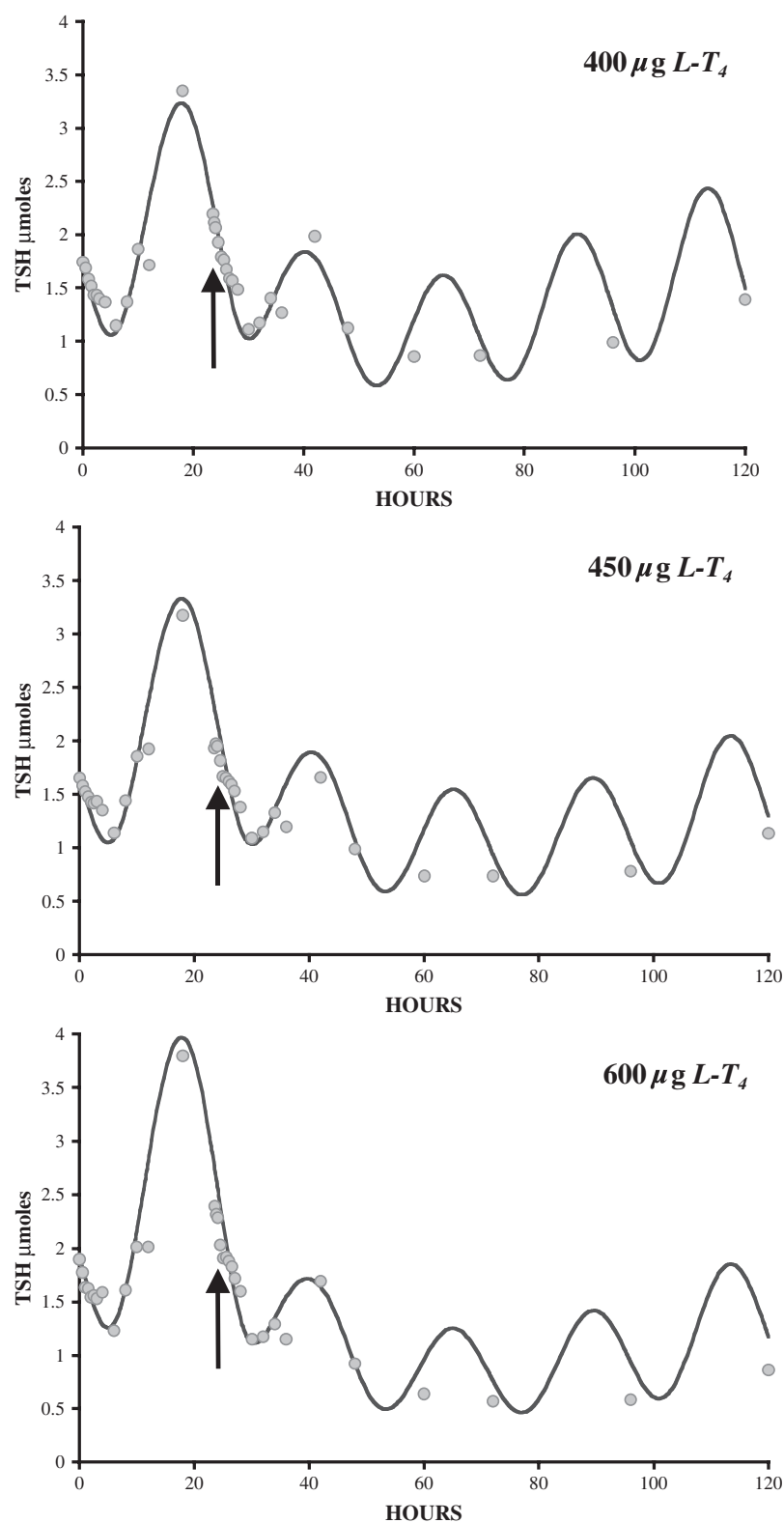


FIG. 5. Optimized brain submodel thyroid-stimulating hormone (TSH(t)) responses fitted simultaneously to data ($n = 33$) from three pharmacokinetic studies using 400, 450, and 600 μg levothyroxine ($L-T_4$) dosing (10). These data also illustrate the nonlinear properties of the TSH-saturating response characteristics, fitted well by the model.

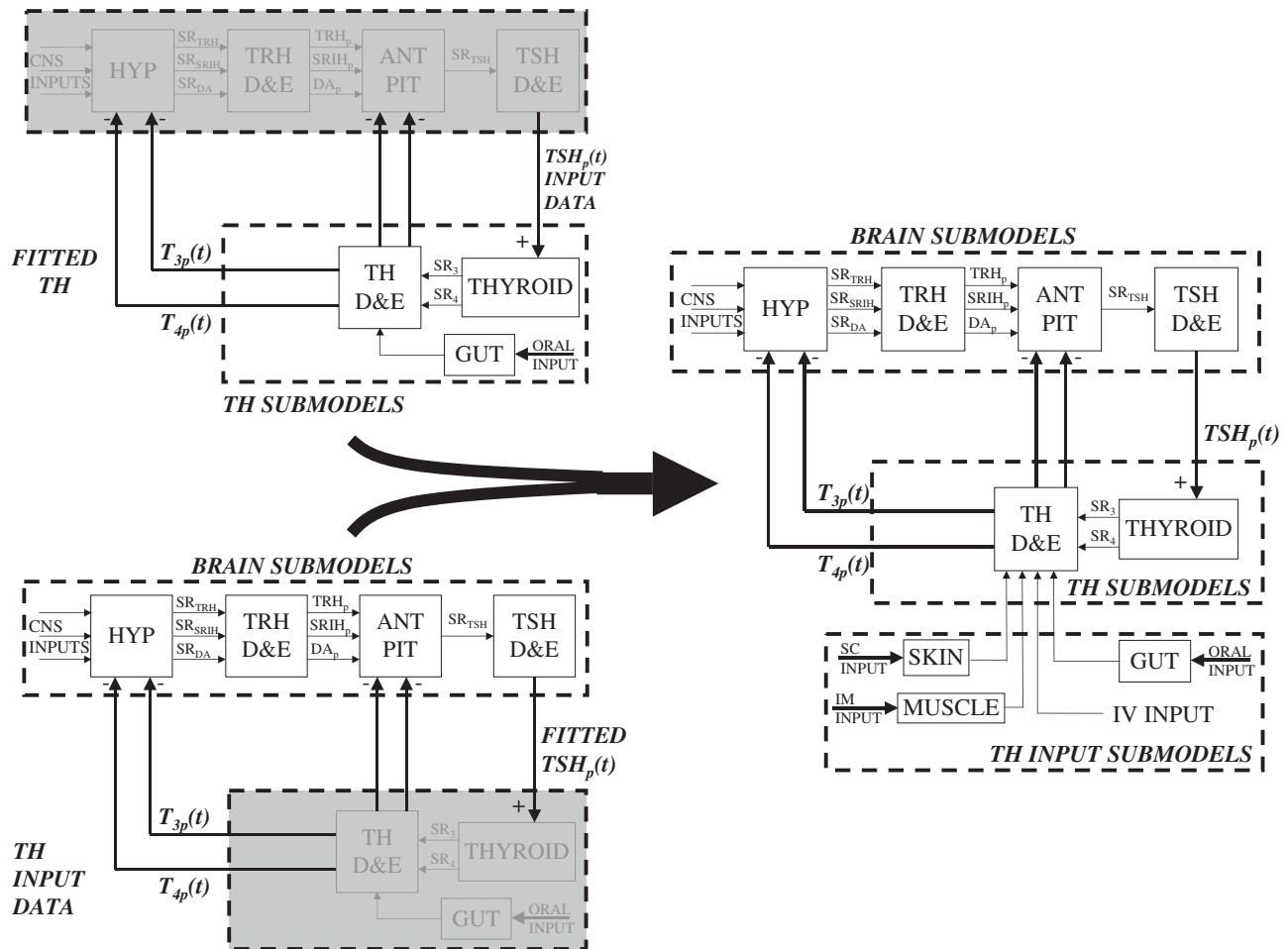


FIG. 6. Brain (bottom left) and thyroid (top left) submodels combined to make the complete feedback control system (FBCS) model (right). Triiodothyronine (T_3), thyroxine (T_4), and thyroid-stimulating hormone (TSH) data used as input forcing functions, with the submodels encompassed and replaced by the input forcing function boxed in gray. The complete FBCS model on the right also includes submodels for subcutaneous (SC), intramuscular (IM), and intravenous (IV) exogenous inputs, used in our clinical applications.

brain submodel, we reversed the roles of the data sets, using T_3 and T_4 plasma discrete-time data (shown as squares in Fig. 4) as input forcing functions, rendered continuous time using linear splines (11), and optimally fitted the new brain submodel to plasma TSH output data (Fig. 6, bottom left). Extensive numerical analyses^b of the brain submodel revealed that all parameters but two are uniquely quantifiable (identifiable) from the data; k_3 and k_4 are not separately quantifiable from our input-output data, which motivated a search for model simplification. Silva and coworkers reported roughly half of TH effect on TSH secretion in steady state due to plasma-derived T_3 , the remainder to plasma-derived T_4 to T_3

conversion in rat pituitary (13–18), and other data suggest a similar relationship in humans (19–23), together implying $k_3 \approx k_4$ in Eq. 2. We fitted the unknown brain submodel parameters (B_0 , A_0 , ϕ_{phase} , k_4 , k_3 , and k_{degT3B} in Eqs. 1 and 2) to the TSH plasma data for all three doses simultaneously. We initiated the search with $k_3 = k_4$ and tested values of k_3 ranging $\pm 30\%$ above and below k_4 . We used the program SAAM II (11) for parameter optimization, as before (1).

Complete FBCS H-P-T axis model

We incorporated the new quantified brain submodels and updated and requantified TH SR and D&E submodels into an overall FBCS simulation model, thereby forming the complete, updated closed-loop FBCS simulation model illustrated in Figure 6. To check whether the combined submodels behave as well in concert as they do individually, we simulated responses of the complete FBCS model to 400, 450, and 600 μg doses of simulated oral L- T_4 and compared these predictions to the simulations by each submodel individually, as well as to the real PK data (10).

^bAn established numerical identifiability analysis approach (12) was used to explore the brain submodel parameter space for feasible solutions with finite parameter estimation variances. A range of physiologically reasonable values for the k 's were tested by generating perfect simulated data for each trial and reestimating the parameters and their variances. Infinite (or very large) variances indicate unidentifiability.

TABLE 1. PARAMETER NOMENCLATURE, UNITS, VALUES, ESTIMATES, VARIABILITIES (%CV), AND SOURCES

Parameter	Estimate	Units	%CV	Submodel	Source
k_{degT3B}	0.037	h^{-1}	12.6	TSH SR	Fitted to Blakesley <i>et al.</i> (10) data
ϕ_{phase}	-3.71	h^{-1}	1.04	TSH SR	Fitted to Blakesley <i>et al.</i> (10) data
A_0	581	$\mu\text{mol/h}$	61.4	TSH SR	Fitted to Blakesley <i>et al.</i> (10) data
B_0	1166	$\mu\text{mol/h}$	60.7	TSH SR	Fitted to Blakesley <i>et al.</i> (10) data
$k_3 = k_4$	0.118	$\mu\text{mol/h}$	6.43	TSH SR	Fitted to Blakesley <i>et al.</i> (10) data
k_{degTSH}	0.756	h^{-1}	—	TSH D&E	Ridgway <i>et al.</i> (5), Odell <i>et al.</i> (4), Kuku <i>et al.</i> (3)
V_{dTSH}	3.5	L	—	TSH D&E	Ridgway <i>et al.</i> (5), Odell <i>et al.</i> (4), Kuku <i>et al.</i> (3)
V_{p}	3	L	—	TH D&E	
K_{mD1fast}	0.03	μmol	—	TH D&E	Updated by [Sharifi and St. Germain (7), Goswami and Rosenberg (8)]
K_{mD1slow}	1.0	μmol	—	TH D&E	Updated by [Sharifi and St. Germain (7), Goswami and Rosenberg (8)]
K_{mD2slow}	0.075	μmol	—	TH D&E	Bianco <i>et al.</i> (9)
$V_{\text{maxD1fast}}$	3.85×10^{-4}	h^{-1}	30.6	TH D&E	Refitted to Blakesley <i>et al.</i> (10) data
$V_{\text{maxD1slow}}$	6.63×10^{-4}	h^{-1}	6.27	TH D&E	Refitted to Blakesley <i>et al.</i> (10) data
$V_{\text{maxD2slow}}$	0.00109	h^{-1}	6.27	TH D&E	Refitted to Blakesley <i>et al.</i> (10) data
S_3	3.71×10^{-4}	μmol^{-1}	6.49	TH SR	Refitted to Blakesley <i>et al.</i> (10) data
S_4	0.00168	μmol^{-1}	7.4	TH SR	Refitted to Blakesley <i>et al.</i> (10) data
gut1	1.3	h^{-1}	—	T ₄ GUT	DiStefano and Mak (26)
gut2	0.119	h^{-1}	16.3	T ₄ GUT	DiStefano and Mak (26) refitted to Blakesley <i>et al.</i> (10) data
gut3	0.881	h^{-1}	2.2	T ₄ GUT	DiStefano and Mak (26) refitted to Blakesley <i>et al.</i> (10) data
k_{T3absorp}	0.882	h^{-1}	7.2	T ₃ GUT	Fitted to Ueda <i>et al.</i> (25) data
k_{T3deg}	0.118	h^{-1}	7.2	T ₃ GUT	Fitted to Ueda <i>et al.</i> (25) data
k_{T3dissol}	1.78	h^{-1}	32.0	T ₃ GUT	Fitted to Ueda <i>et al.</i> (25) data
k_{SC}	0.034	h^{-1}	—	SC INPUT	Hays (27)
k_{IM}	0.068	h^{-1}	—	IM INPUT	Hays (27)

Only the new brain submodel and updated TH D& E submodel parameters are shown here; the remaining 22 are in Table 1 of Ref. (1). TSH, thyroid-stimulating hormone; SR, secretion; D&E, distribution and elimination; TH, thyroid hormone; T₄, thyroxine; T₃, triiodothyronine; SC, subcutaneous; IM, intramuscular, %CV = coefficient of variation = $100 \times \frac{\text{standard deviation}}{\text{parameter value}}$.

Model validation

We further tested the new FBSC model against a variety of clinical data sets (20,24,25) not used in its development. These included

1. *Normal and abnormal steady-state hormone levels:* We simulated steady-state plasma T_{3pss}, T_{4pss}, and TSH_{pss} concentrations in normal healthy subjects, and in thyroidectomized patients treated with L-T₄, and compared the corresponding simulated hormone concentrations to real clinical data (10,20).

2. *Normal circadian TSH data:* We simulated normal (unperturbed) steady-state plasma T_{3p}(*t*), T_{4p}(*t*), and TSH_p(*t*) responses over 24 hours and compared these to corresponding data collected from normal subjects (24).

3. *Predicting the TSH response to oral T₃ dosing:* Validation of FBSC responses to oral T₃ required an additional gut absorption submodel, to represent pathway dynamics from an exogenous oral T₃ input into the T₃ plasma pool shown in Figure 3. We adapted a T₃ absorption model (1,26) to compute the T₃ absorption and dissolution rates, assumed unknown, by fitting this submodel to time-course plasma T₃ data taken in normal subjects after 75 μg oral T₃ (25). Using the complete FBSC model augmented with the T₃ absorption submodel, we then compared simulated TSH_p(*t*) responses to simulated 75 μg oral T₃ and compared these results predictively to real TSH PK data (25) after the same dose. We emphasize here that the TSH PK data were not used for

quantifying the T₃ absorption rate, but only for predictive validation purposes.

Methods II: Clinical Applications of the Simulator

Combined T₃/T₄ treatment—updated

We expanded the simulation study done earlier with the simpler TH submodel alone (1), now using the updated and complete FBSC H-P-T axis model. We recomputed the L-T₄—only doses needed to normalize (a) plasma T₃, (b) lumped-tissue T₃ levels (from Fig. 3), and (c) a combined T₃ and T₄ regimen that approximately normalizes both plasma and lumped-tissue T₃ levels. With the updated and more complete model, we were able to simulate plasma TSH(*t*) responses as well as update our earlier plasma T₃ and T₄ predictions.

Parenteral T₄ administration

Following the lead of Hays (27), we simulated subcutaneous (SC) and intramuscular (IM) administration of L-T₄, using simple one-compartment models with an absorption half-life of 20.4 hours for SC administration, and an IM absorption rate twice that of SC (27,28)—rate constants $k_{\text{SC}} = \ln 2/20.4 = 0.034 \text{ h}^{-1}$ and $k_{\text{IM}} = 0.068 \text{ h}^{-1}$; see Figure 6. We computed the simulated L-T₄ dose needed to normalize lumped-tissue T₃ levels, when administered once or twice weekly, and either subcutaneously or intramuscularly. We also simulated plasma T₃, T₄, and TSH responses to each of these four regimens.

TABLE 2. COMPARISON OF OPTIMUM PARAMETER ESTIMATES FOR OUR ORIGINAL THYROID SUBMODELS (1) WITH OPTIMUM ESTIMATES USING THE UPDATED D1 K_m 20 nM

Parameter	Original thyroid submodels		Updated thyroid submodels		% Change from orig. estimate ^a
	Estimate	%CV	Estimate	%CV	
τ	6 h		8 h		+33
D1 K_m	1.9 μ M	—	20 nM	—	−98.9
D2 K_m	1.5 nM	—	1.5 nM	—	0.00
D1 V_{\max} fast pool	0.00999 h^{-1}	10.44	0.000385 h^{-1}	30.6	−96.1
D1 V_{\max} slow pool	0.0279 h^{-1}	7.87	0.000663 h^{-1}	6.27	−97.6
D2 V_{\max} slow pool	0.000746 h^{-1}	7.87	0.00109 h^{-1}	6.27	+46.1
S_3	0.000336 h^{-1}	4.33	0.000371 h^{-1}	6.49	+10.4
S_4	0.00174 h^{-1}	7.21	0.00168 h^{-1}	7.4	−3.45
T_4 absorption rate	0.882 h^{-1}	2.23	0.881 h^{-1}	2.2	0.00

^a%Change = $100 \times (\text{new estimate} - \text{old estimate}) / \text{old estimate}$.

Central hypothyroidism

We simulated secondary hypothyroidism by first decreasing the magnitude of the sinusoid (A_0) in the TSH secretion rate equation (Eq. 1) to 25% of normal, thereby decreasing the nighttime TSH surge, as is often seen in central hypothyroidism (29). Additionally, we decreased the overall TSH secretion rate (SR_{TSH}) to 50%, 25%, 10%, 1%, and 0.1% of normal to simulate varying levels of secondary hypothyroidism.

Results

Brain submodel quantification

Numerical testing of the brain submodel parameters $k_3 \approx k_4$ constraint for Eq. 2 yielded very similar fits and parameter estimates for values of k_3 30% above and below k_4 (or vice versa), so $k_3 = k_4$ in further simulations presented here. Figure 5 shows optimized plasma TSH(t) outputs for the new brain submodel, compared with TSH PK data. These were optimized by simultaneous fitting of data from experiments done with all three L- T_4 doses, to capture the nonlinearities, using T_3 and T_4 input forcing functions. Optimized parameter estimates and statistics for the brain submodel are given in Table 1.

Thyroid submodels—effects of deiodinase K_m values on model precision and predictive value

K_{mD1} update Optimum parameter estimates of the original and updated models are compared in Table 2. The estimated D1 V_{\max} values in both fast and slow tissue pools fell roughly 100-fold, paralleling the change in K_{mD1} to 20 nM. The time-delay estimate τ for the thyroidal secretion responses to TSH stimulation that yielded the best fit to the data (Fig. 4) was centered at 8 hours, compared with 6 hours previously. A 6- to 8-hour range gave nearly identical results in both models, a range supported by several studies (30–33), as well as our own data in Figures 4 and 5.

D2 with T_4 estimate of V_{\max} in the slow pool increased 46%. The TH secretion “gain” parameters changed 3–10%, and the remaining parameter estimates were unchanged. The quality of the model fitted to the data was essentially unchanged with the updated submodel included, as established from program optimization criteria, which were essentially the same for both

models,^c and illustrated in Figure 4. Reevaluation of earlier model predictions indicated no changes to our previous bioequivalence and replacement hormone results (1).

K_{mD2} sensitivities Newly optimized TH D&E and SR submodel parameter estimates for ± 10 -fold and ± 100 -fold changes in K_m values used for D2 with T_4 are given in Table 3. Small differences in several optimum parameter estimates are noted, but these had negligible effects on the weighted residual sum of squares (Table 3) and primary model predictions. For this reason, we retain the original $K_{mD2}(T_4)$ in the new model.

Complete FBCS H-P-T axis model

Aggregation of submodels Simulation of plasma $T_{3p}(t)$, $T_{4p}(t)$, and $TSH_p(t)$ responses to 400, 450, and 600 μ g L- T_4 dosing using the complete FBCS model was essentially indistinguishable from optimized simulation responses to the same inputs by individual submodels shown in Figures 4 and 5. All model equations and parameter values are given together in the Appendix.

Model validation

1. **Steady-state hormone level predictions:** Comparisons of simulated steady-state hormone levels for normal subjects and treated thyroidectomized patients versus real steady-state hormone data are shown in Figure 7. Simulated results were nearly identical to measured steady-state hormone concentrations in patients from our primary database and matched clinical range data very well, both as shown in Figure 7.

2. **Predicting normal circadian TSH data:** Predicted normal TSH circadian rhythms matched measured data (24) well, as shown in Figure 8.

3. **Predicting TSH response to T_3 dosing:** Resulting T_3 absorption was 88% and dissolution 1.78 h^{-1} when fitted to T_3 plasma data (Fig. 9A). Gut parameter estimation results are

^cTwo model comparison measures were used: the Akaike Information Criterion (AIC: −0.83 vs. −0.89) and the optimization criterion function (−3.6 vs. −3.7), for the updated and original submodels, both reported in SAAM II optimization results (11).

TABLE 3. SENSITIVITIES OF OPTIMAL MODEL PARAMETER ESTIMATES FOR THE THYROID AND TH D&E SUBMODELS TO $\pm 10\%$ AND $\pm 100\%$ VARIATIONS IN $D2 K_m(T_4)$

Parameter	$D2 K_m + 100\%$			$D2 K_m + 10\%$			Original $D2 K_m$ est.			$D2 K_m - 10\%$			$D2 K_m - 100\%$		
	Estimate	%CV		Estimate	%CV		Estimate	%CV		Estimate	%CV		Estimate	%CV	
τ	8 h	—		8 h	—		8 h	—		8 h	—		8 h	—	
$D1 K_m$	20 nM	—		20 nM	—		20 nM	—		20 nM	—		20 nM	—	
$D2 K_m$	15 nM	—		15 nM	—		15 nM	—		15 nM	—		15 nM	—	
$D1 V_{max}$ fast pool	0.00241 h ⁻¹	59.3		0.00264 h ⁻¹	49.3		0.00385 h ⁻¹	30.6		0.00419 h ⁻¹	27.6		0.00423 h ⁻¹	27.3	
$D1 V_{max}$ slow pool	0.00582 h ⁻¹	7.20		0.00636 h ⁻¹	6.55		0.00663 h ⁻¹	6.27		0.00666 h ⁻¹	6.25		0.00666 h ⁻¹	6.25	
$D2 V_{max}$ slow pool	0.0121 h ⁻¹	7.20		0.00214 h ⁻¹	6.55		0.00109 h ⁻¹	6.27		0.000974 h ⁻¹	6.25		0.000963 h ⁻¹	6.25	
S_3	0.00452 h ⁻¹	7.07		0.00422 h ⁻¹	6.58		0.00371 h ⁻¹	6.49		0.00359 h ⁻¹	6.53		0.00357 h ⁻¹	6.53	
S_4	0.00160 h ⁻¹	7.90		0.00162 h ⁻¹	7.71		0.00168 h ⁻¹	7.4		0.00169 h ⁻¹	7.33		0.00169 h ⁻¹	7.32	
T_4 absorption rate	0.880 h ⁻¹	2.20		0.880 h ⁻¹	2.20		0.881 h ⁻¹	2.2		0.881 h ⁻¹	2.20		0.881 h ⁻¹	2.20	
Total objective	—	—	-3.72	—	—	-3.78	—	—	-3.81	—	—	-3.81	—	—	-3.81

T_4 , thyroxine.

given in Table 1. The predicted $TSH_p(t)$ response to oral T_3 closely matched measured plasma TSH data, as shown in Figure 9B.

Simulator clinical applications

Updated combined T_3/T_4 treatment The simulated L- T_4 -only dose needed to normalize plasma T_3 to pre-thyroidectomy levels was 165 μ g L- T_4 /day, the L- T_4 -only dose needed to normalize lumped-tissue T_3 levels was 145 μ g L- T_4 /day, and the combined L- T_4 + T_3 dose needed to normalize both plasma and lumped-tissue T_3 levels (as well as plasma T_4 levels) was 105 μ g L- T_4 + 9 μ g T_3 per day. In all three regimens, average steady-state-simulated plasma T_3 , T_4 , and TSH were all within their normal ranges (T_4 : 5–12 μ g/dL; T_3 : 0.8–1.9 ng/mL; and TSH: 0.5–5 mU/L).

Parenteral T_4 administration Lumped-tissue T_3 levels were roughly normalized using simulated dosings of 800 μ g L- T_4 weekly and 400 μ g twice weekly, for both the SC and IM routes, similar to the 750 and 375 μ g reported by Hays (27). In all four regimens (once vs. twice weekly, SC vs. IM), plasma T_3 , T_4 , and mean TSH were maintained within their normal ranges (T_4 : 5–12 μ g/dL; T_3 : 0.8–1.9 ng/mL; and TSH: 0.5–5 mU/L). Once weekly, IM administration of L- T_4 showed the largest fluctuation in plasma TSH levels, with nighttime peaks as high as 8 mU/L near the end of the week; twice weekly, SC administration by contrast showed the smallest fluctuation in TSH plasma levels, which stayed within 1.5–4.5 mU/L.

Central hypothyroidism Results for TSH secretion suppression ranging from 0.1% to 50% of normal are given in Figure 10. Steady-state plasma TSH levels stayed (barely) within the normal range throughout the simulations, though plasma T_4 dropped below the normal range as TSH secretion was reduced below 25%, and plasma T_3 dropped below the normal range below 1% TSH secretion. As expected, time-course plasma TSH dropped rapidly after reducing TSH secretion, due to its relatively short half-life in blood. This was followed by a slow return of TSH toward normal, due to relatively slower TH negative feedback response dynamics, all as shown in the inset in Figure 10.

Discussion

New simulator development and validation

We built this model on the framework established by Eisenberg *et al.* (1), the major update being explicit representation and quantification of the brain submodels not included earlier. The new simulator incorporates circadian and basal TSH secretion, as well as nonlinear T_3 and T_4 regulation of TSH secretion and—for the first time—it has been fully quantified from a substantial quantity of clinical data, over a wide range of physiological and pathophysiological conditions. Earlier FBCS models of thyroid hormone regulation were similarly structured [e.g., Refs. (34–39)], but severely encumbered by lack of quantitative data for model building or verification.

We quantified the brain submodels using physiological and PK data and combined these new submodels with our updated TH submodels, thereby providing a quantified

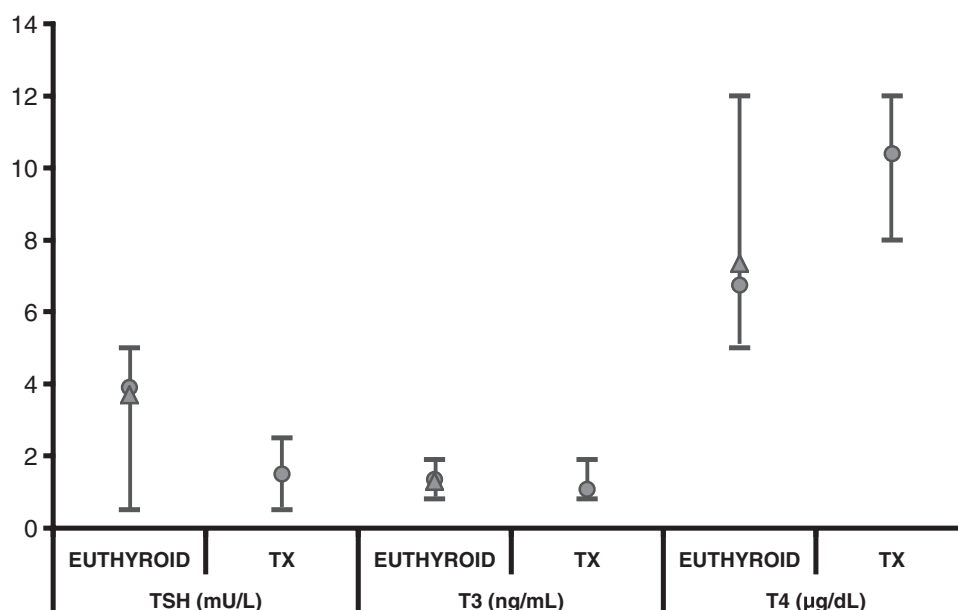


FIG. 7. Feedback control system model validation study results. Predicted steady-state concentrations of thyroid-stimulating hormone (TSH), triiodothyronine (T_3), and thyroxine (T_4) in normal euthyroids and thyroidectomized patients treated with 150 μg levothyroxine ($L-T_4$) (circles) versus steady-state hormone data (triangles) (10) and typical clinical ranges (bars) (20).

simulation model of the complete closed-loop system. The nonlinear TH D&E submodel was updated with a more physiological deiodinase K_m value (7), which did not affect the fit of the model to the data, but did alter the relative amounts of T_4 converted to T_3 in slow versus fast tissues. The extended simulation model, with $TSH(t)$ now included as a response variable, is capable of exploring many more physiological and clinical conditions; it no longer requires specific, case-by-case experimental TSH data.

We did not include ultradian TSH oscillations in our model because apparent smoothing characteristics of downstream

thyroid gland and D&E components likely damp out any effects of these oscillations on feedback regulation. Further, as ultradian rhythms are not in phase between individuals, our model—which is based on the dynamics of a subject population average—further smooths these smaller variations.

We validated the new FBCS model by independent comparisons with data not used in its development. Simulated steady-state plasma T_3 , T_4 , and TSH concentrations in euthyroids and treated thyroidectomized patients were well within normal ranges and also closely matched normal steady-state data from actual subjects (10). In treated thyroidectomized (open-loop) patients, steady-state T_3 and T_4 predictions were nearly identical to our previous simulation results (1). Normal daily $TSH_p(t)$ circadian variation simulations also closely matched independent plasma TSH data taken from normal human subjects (24) (Fig. 8); and simulated normal daily T_3 and T_4 showed circadian variation of smaller magnitude, consistent with clinical data for human subjects (20,40).

We also validated the complete FBCS model against independent TSH response data following an oral T_3 challenge (25). T_3 dissolution and absorption into plasma from gut was modeled using a two-compartment gut T_3 submodel and quantified from T_3 plasma appearance data after 75 μg oral T_3 (25). This test was important because, while effects of T_3 on TSH secretion are explicit in the brain submodel, the overall FBCS model was optimized only to T_4 response data, not T_3 . Simulated plasma $TSH_p(t)$ response to an oral 75 μg T_3 dose matched real TSH data quite closely (Fig. 9), providing independent validation for the previously untested T_3 regulatory pathway of the model.

Simulator applications

Combined T_3/T_4 treatment—updated In simulated thyroidectomized subjects, we found 165 μg $L-T_4$ /day normal-

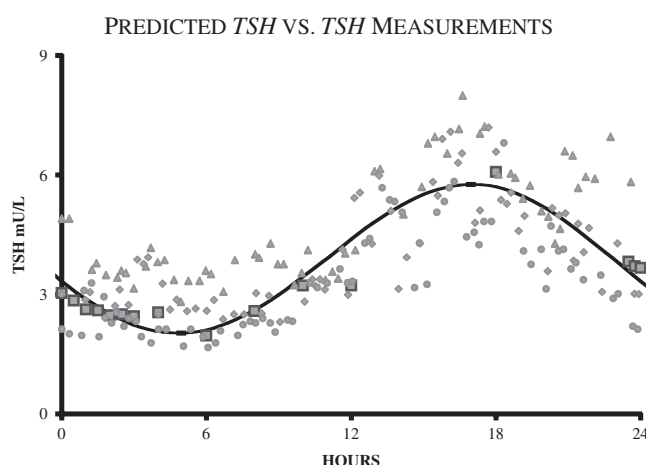


FIG. 8. Feedback control system (FBCS) model validation study results. Predicted normal circadian thyroid-stimulating hormone (TSH) versus independent TSH data (not used in fitting the FBCS model) from three individuals [triangles and diamonds from (24), circles from (42)]. Also shown (squares) are the mean TSH data from the larger database used to fit the FBCS model (10).

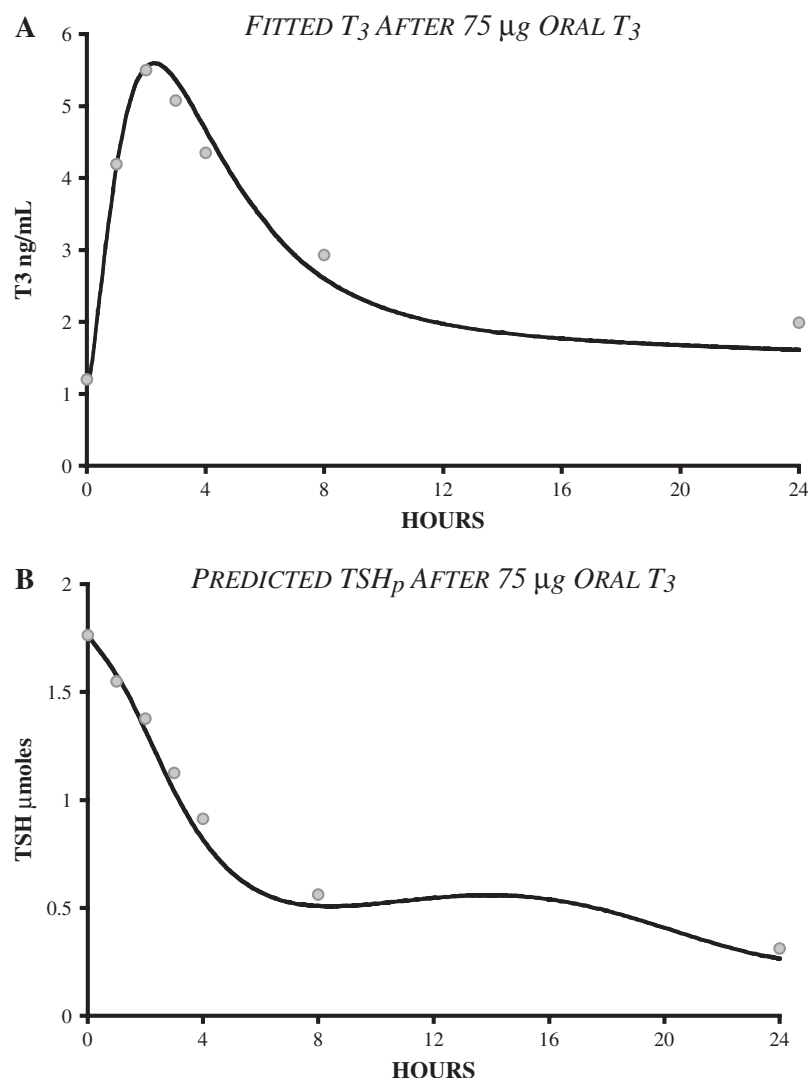


FIG. 9. (A) Fit of additional triiodothyronine (T₃) absorption model to T₃ data ($n = 28$) taken after 75 µg oral T₃ (25). T₃ absorption was fit to 88%. (B) Feedback control system model validation study results. Predicted thyroid-stimulating hormone (TSH) concentrations in normal subjects after 75 µg oral T₃, compared with TSH data from (25), following same input.

ized plasma T₃, 145 µg L-T₄/day normalized lumped-tissue T₃, and 105 µg L-T₄ + 9 µg T₃ per day normalized both plasma and lumped-tissue T₃ levels, as well as plasma T₄ levels. All three regimens are quite close to our earlier simulation predictions (1) of 162 µg L-T₄/day, 141 µg L-T₄/day, and 103 µg L-T₄/day + 6 µg T₃/day, respectively. And all three regimens maintained plasma TSH, T₃, and T₄ within normal ranges. Previously, we had compared combined L-T₄ + T₃ therapy versus L-T₄-only therapy, by simulating T₃ levels only in tissue and plasma, without the benefit of a closed feedback loop (1). We had no explicit model of the H-P brain components, so we could not simulate corresponding plasma TSH levels.

Interestingly, the daily TSH circadian range—from nighttime peak to daytime nadir—was somewhat higher (2.3–5.0 mU/L) with combined T₃/T₄ treatment versus 0.5–1.3 and 1.1–2.7 mU/L for the two L-T₄-only regimens. The combined treatment circadian range more closely matches our simulations and clinical data for euthyroid normal subjects (~2–6 mU/L; see Figs. 8 and 5), but all three regimens maintained TSH levels within the normal range. This effect is likely due to high-normal T₄ levels, observed both in our simulations and

in patients undergoing L-T₄-only therapy (20), providing additional TSH suppression. These results may serve to explain clinical observations that euthyroid patients on L-T₄-only therapy were subjectively more content when their TSH was low-normal (41)—the simulated T₄-only regimen that normalizes tissue T₃ levels yields a lower average TSH concentration than our normal subject simulations and data.

Parenteral T₄ administration We confirmed and expanded on Hays' recent analysis of these alternate drug administration routes (27). Simulated 800 µg L-T₄ weekly and 400 µg L-T₄ twice weekly (by SC or IM routes) normalized lumped-tissue T₃ levels, only slightly higher than Hays' results (750 µg L-T₄ once and 375 µg L-T₄ twice weekly). Whereas Hays used only T₄ subsystem kinetics, we were able to simulate TSH and T₃ as well, finding that daily average plasma TSH as well as T₃ and T₄ remained within normal ranges for all four dosing scenarios. These simulations provide further evidence that L-T₄ can be administered parenterally once or twice weekly in patients with diminished L-T₄ gut absorption, maintaining TSH and TH levels in blood and tissues within normal ranges.

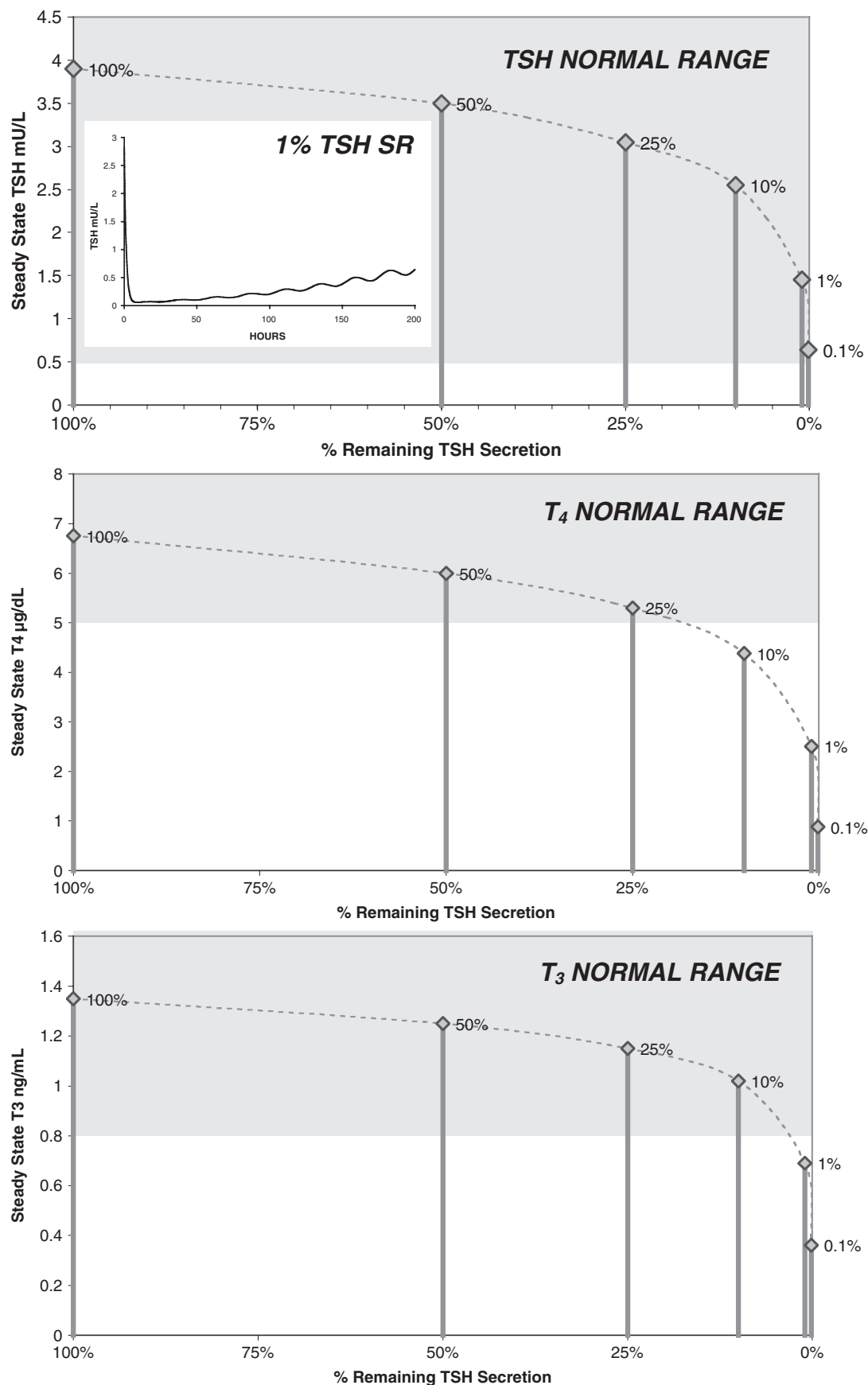


FIG. 10. Effects of central hypothyroidism on steady-state thyroid-stimulating hormone (TSH), thyroxine (T_4), and triiodothyronine (T_3). Hormone levels versus TSH secretion at 100%, 50%, 25%, 10%, 1%, and 0.1% of normal. Inset (top): Predicted time-course of plasma TSH response to reducing TSH secretion to 1% of normal at $t=0$. Grey shading indicates normal range for each hormone.

Central hypothyroidism Steady-state hormone concentrations in response to various degrees of central hypothyroidism (Fig. 10) were within normal ranges for TSH secretion down to 25% of normal. Simulated TSH levels showed an initial drop to nearly zero (see Fig. 10) immediately after reducing TSH secretion, before returning toward normal, illustrating the powerful feedback effects at work, even when TSH secretion is greatly diminished.

IN SUMMARY, we have demonstrated that the new simulator captures the essential features of H-P-T axis dynamics over a fairly wide range of linear and nonlinear operation, both physiological and pathophysiological. Independent validation against data not used in model development suggests that it is capable of accurate predictions and it is thus potentially useful for exploring other unanswered questions about TH regulation in health and disease.

Acknowledgments

This project was supported in part by a Howard Hughes Medical Institute grant through the Undergraduate Biological Sciences Education Program to UCLA, the UCLA Graduate Research Mentorship Fellowship, and the National Institutes of Health National Research Service Award (T32-GM008185) from the National Institute of General Medical Sciences (NIGMS).

Disclosure Statement

No competing financial interests exist.

References

- Eisenberg M, Samuels M, DiStefano JJ, 3rd 2006 L-T4 bioequivalence and hormone replacement studies via feedback control simulations. *Thyroid* **16**:1279–1292.
- Samuels MH, Henry P, Luther M, Ridgway EC 1993 Pulsatile TSH secretion during 48-hour continuous TRH infusions. *Thyroid* **3**:201–206.
- Kuku SF, Harsoulis P, Kjeld M, Fraser TR 1975 Human thyrotropic hormone kinetics and effects in euthyroid males. *Horm Metab Res* **7**:54–59.
- Odell WD, Utiger RD, Wilber JF, Condliffe PG 1967 Estimation of the secretion rate of thyrotropin in man. *J Clin Invest* **46**:953–959.
- Ridgway EC, Weintraub BD, Maloof F 1974 Metabolic clearance and production rates of human thyrotropin. *J Clin Invest* **53**:895–903.
- Visser TJ, Kaptein E, Terpstra OT, Krenning EP 1988 Deiodination of thyroid hormone by human liver. *J Clin Endocrinol Metab* **67**:17–24.
- Sharifi J, St. Germain DL 1992 The cDNA for the type I iodothyronine 5'-deiodinase encodes an enzyme manifesting both high Km and low Km activity. Evidence that rat liver and kidney contain a single enzyme which converts thyroxine to 3,5,3'-triiodothyronine. *J Biol Chem* **267**:12539–12544.
- Goswami A, Rosenberg IN 1988 Effects of glutathione on iodothyronine 5'-deiodinase activity. *Endocrinology* **123**:192–202.
- Bianco AC, Salvatore D, Gereben B, Berry MJ, Larsen PR 2002 Biochemistry, cellular and molecular biology, and physiological roles of the iodothyronine selenodeiodinases. *Endocr Rev* **23**:38–89.
- Blakesley VA, Awni W, Locke C, Ludden TM, Granneman GR, Braverman LE 2004 Are bioequivalence studies of levothyroxine sodium formulations in euthyroid volunteers reliable? *Thyroid* **14**:191–200.
- Barrett PH, Bell BM, Cobelli C, Golde H, Schumitzky A, Vicini P, Foster DM 1998 SAAM II: simulation, analysis, and modeling software for tracer and pharmacokinetic studies. *Metabolism* **47**:484–492.
- Jaquez JA, Greif P 1985 Numerical parameter identifiability and estimatability: integrating identifiability, estimatability, and optimal sampling design. *Math Biosci* **77**:201–227.
- Larsen PR 1982 Thyroid-pituitary interaction: feedback regulation of thyrotropin secretion by thyroid hormones. *N Engl J Med* **306**:23–32.
- Larsen PR, Bavli SZ, Castonguay M, Jove R 1980 Direct radioimmunoassay of nuclear 3,5,3' triiodothyronine in rat anterior pituitary. *J Clin Invest* **65**:675–681.
- Silva JE, Larsen PR 1978 Contributions of plasma triiodothyronine and local thyroxine monodeiodination to triiodothyronine to nuclear triiodothyronine receptor saturation in pituitary, liver, and kidney of hypothyroid rats. Further evidence relating saturation of pituitary nuclear triiodothyronine receptors and the acute inhibition of thyroid-stimulating hormone release. *J Clin Invest* **61**:1247–1259.
- Larsen PR 1981 Regulation of thyrotropin secretion by 3,5,3'-triiodothyronine and thyroxine. *Prog Clin Biol Res* **74**:81–93.
- Larsen PR, Silva JE, Kaplan MM 1981 Relationships between circulating and intracellular thyroid hormones: physiological and clinical implications. *Endocr Rev* **2**:87–102.
- Silva JE, Larsen PR 1977 Pituitary nuclear 3,5,3'-triiodothyronine and thyrotropin secretion: an explanation for the effect of thyroxine. *Science* **198**:617–620.
- Bigos ST, Ridgway EC, Kourides IA, Maloof F 1978 Spectrum of pituitary alterations with mild and severe thyroid impairment. *J Clin Endocrinol Metab* **46**:317–325.
- DeGroot LJ, Hennemann G 2002 Thyroid disease manager: the thyroid and its diseases. <http://www.thyroidmanager.org/thyroidbook.htm>. Accessed September 2004.
- Patel YC, Burger HG 1973 Serum triiodothyronine in health and disease. *Clin Endocrinol (Oxf)* **2**:339–349.
- Patel YC, Pharoah PO, Hornabrook RW, Hetzel BS 1973 Serum triiodothyronine, thyroxine and thyroid-stimulating hormone in endemic goiter: a comparison of goitrous and nongoitrous subjects in New Guinea. *J Clin Endocrinol Metab* **37**:783–789.
- Wennlund A 1986 Variation in serum levels of T3, T4, FT4 and TSH during thyroxine replacement therapy. *Acta Endocrinol (Copenh)* **113**:47–49.
- Sarapura VD, Samuels MH, Ridgway EC 2002 Thyroid-stimulating hormone. In: Melmed S (ed) *The Pituitary*. Second edition. Blackwell Science, Malden, MA, pp 187–229.
- Ueda S, Takamatsu J, Fukata S, Tanaka K, Shimizu N, Sakata S, Yamaji T, Kuma K, Ohsawa N 1996 Differences in response of thyrotropin to 3,5,3'-triiodothyronine and 3,5,3'-triiodothyroacetic acid in patients with resistance to thyroid hormone. *Thyroid* **6**:563–570.
- DiStefano JJ, 3rd, Mak PH 1979 On model and data requirements for determining the bioavailability of oral therapeutic agents: application to gut absorption of thyroid hormones. *Am J Physiol* **236**:R137–R141.
- Hays MT 2007 Parenteral thyroxine administration. *Thyroid* **17**:127–129.
- Hays MT, McGuire RA 1980 Distribution of subcutaneous thyroxine, triiodothyronine, and albumin in man: comparison

- with intravenous administration using a kinetic model. *J Clin Endocrinol Metab* **51**:1112–1117.
29. Samuels MH, Lillehei K, Kleinschmidt-Demasters BK, Stears J, Ridgway EC 1990 Patterns of pulsatile pituitary glycoprotein secretion in central hypothyroidism and hypogonadism. *J Clin Endocrinol Metab* **70**:391–395.
 30. Huysmans DA, Nieuwlaet WA, Erdtsieck RJ, Schellekens AP, Bus JW, Bravenboer B, Hermus AR 2000 Administration of a single low dose of recombinant human thyrotropin significantly enhances thyroid radioiodide uptake in nontoxic nodular goiter. *J Clin Endocrinol Metab* **85**:3592–3596.
 31. Nielsen VE, Bonnema SJ, Hegedus L 2004 Effects of 0.9 mg recombinant human thyrotropin on thyroid size and function in normal subjects: a randomized, double-blind, cross-over trial. *J Clin Endocrinol Metab* **89**:2242–2247.
 32. Ramirez L, Braverman LE, White B, Emerson CH 1997 Recombinant human thyrotropin is a potent stimulator of thyroid function in normal subjects. *J Clin Endocrinol Metab* **82**:2836–2839.
 33. Torres MS, Ramirez L, Simkin PH, Braverman LE, Emerson CH 2001 Effect of various doses of recombinant human thyrotropin on the thyroid radioactive iodine uptake and serum levels of thyroid hormones and thyroglobulin in normal subjects. *J Clin Endocrinol Metab* **86**:1660–1664.
 34. Dietrich JW, Tesche A, Pickardt CR, Mitzdorf U 2002 Fractal properties of the thyrotropic feedback control implications of a nonlinear model compared with empirical data. In: Trapp R (Ed) *Cybernetics and Systems*. Austrian Society for Cybernetic Studies, Vienna, pp 329–34.
 35. Dietrich JW, Tesche A, Pickardt CR, Mitzdorf U 2004 Thyrotropic feedback control: evidence for an additional ultrashort feedback loop from fractal analysis. *Cybern Syst* **35**:315–331.
 36. DiStefano JJ, 3rd, Stear EB 1968 Neuroendocrine control of thyroid secretion in living systems: a feedback control system model. *Bull Math Biophys* **30**:3–26.
 37. DiStefano JJ, 3rd, Stear EB 1968 On identification of hypothalamo-hypophysial control and feedback relationships with the thyroid gland. *J Theor Biol* **19**:29–50.
 38. Li G, Liu B, Liu Y 1995 A dynamical model of the pulsatile secretion of the hypothalamo-pituitary-thyroid axis. *Biosystems* **35**:83–92.
 39. Liu YW, Liu BZ, Xie JL, Liu YX 1994 A new mathematical model of hypothalamo-pituitary-thyroid axis. *Math Comput Model* **19**:81–90.
 40. Fisher DA 1996 Physiological variations in thyroid hormones: physiological and pathophysiological considerations. *Clin Chem* **42**:135–139.
 41. Green WL 2005 New questions regarding bioequivalence of levothyroxine preparations: a clinician's response. *AAPS J* **7**:E54–E58.
 42. Samuels M, Luther M, Hentry P, Ridgway EC 1994 Effects of hydrocortisone on pulsatile pituitary glycoprotein secretion. *JCEM* **76**:211–215.

Address reprint requests to:

Marisa Eisenberg, MS

Biocybernetics Laboratory

Departments of Computer Science

Medicine, and Biomedical Engineering

UCLA

Los Angeles, CA 90095-1596

E-mail: marisa@cs.ucla.edu

Appendix

Brain submodel equations (see Methods section)

$$SR_{TSH}(t) = (B_0 + A_0 \sin(\frac{2\pi}{24}t - \phi_{\text{phase}}))e^{-T_{3B}(t)} \quad \text{Eq. 1}$$

$$\dot{TSH}_p = SR_{TSH} - k_{\text{degTSH}}TSH_p \quad \text{See TSH D\&E submodel in Methods}$$

$$\dot{T}_{3B}(t) = \frac{k_4}{T_{4pSS}}T_{4p}(t) + \frac{k_3}{T_{3pSS}}T_{3p}(t) - k_{\text{degT3B}}T_{3B}(t) \quad \text{Eq. 2}$$

Thyroid submodel equations [see Fig. 3 and Ref. (1)]

$$SR_3(t) = S_3TSH(t - \tau) \quad SR_4(t) = S_4TSH(t - \tau) \quad \text{See Fig. 3 and Eq. 6 in Ref (1)}$$

$$\dot{T}_{4p} \equiv \dot{q}_1 = SR_4 + k_{12}q_2 + k_{13}q_3 - (k_{31}^{\text{free}} + k_{21}^{\text{free}})FT_4 + \text{gut3}T_{4\text{dissolv}} + k_{SC}T_{4SC} + k_{IM}T_{4IM} \quad \text{See Fig. 3 and Ref. (1)}$$

$$\dot{q}_2 = k_{21}^{\text{free}}FT_4 - \left(k_{12} + k_{02} + \frac{V_{\text{maxD1fast}}}{K_{mD1fast} + q_2} \right) q_2 \quad \text{See Fig. 3 and Ref. (1)}$$

$$\dot{q}_3 = k_{31}^{\text{free}}FT_4 - \left(k_{13} + k_{03} + \frac{V_{\text{maxD1slow}}}{K_{mD1slow} + q_3} + \frac{V_{\text{maxD2slow}}}{K_{mD2slow} + q_3} \right) q_3 \quad \text{See Fig. 3 and Ref. (1)}$$

$$\dot{T}_{3p} \equiv \dot{q}_4 = SR_3 + k_{45}q_5 + k_{46}q_6 - (k_{64}^{\text{free}} + k_{54}^{\text{free}})FT_3 + k_{T3\text{absorp}}T_{3\text{dissolv}} \quad \text{See Fig. 3 and Ref. (1)}$$

$$\dot{q}_5 = k_{54}^{\text{free}}FT_3 + \frac{V_{\text{maxD1fast}q_2}}{K_{mD1fast} + q_2} - (k_{45} + k_{05})q_5 \quad \text{See Fig. 3 and Ref. (1)}$$

$$\dot{q}_6 = k_{64}^{\text{free}}FT_3 + \frac{V_{\text{maxD1slow}q_3}}{K_{mD1slow} + q_3} + \frac{V_{\text{maxD2slow}q_3}}{K_{mD2slow} + q_3} - (k_{46} + k_{06})q_6 \quad \text{See Fig. 3 and Ref. (1)}$$

$$FT_3 = (a + bT_4 + cT_4^2 + dT_4^3)T_{3p} \quad \text{See Fig. 3 and Eq. 4 in Ref. (1)}$$

$$FT_4 = (A + BT_4 + CT_4^2 + DT_4^3)T_{4p} \quad \text{See Fig. 3 and Eq. 5 in Ref. (1)}$$

Gut and SC/IM input submodels [see Methods and Ref. (1)]

$$\dot{T}_{4\text{solid}} = u_{\text{exog}} - \text{gut1}T_{4\text{solid}} \quad \text{See Methods and Ref. (1)}$$

$$\dot{T}_{4\text{dissolv}} = \text{gut1}T_{4\text{solid}} - (\text{gut2} + \text{gut3})T_{4\text{dissolv}} \quad \text{See Methods and Ref. (1)}$$

$$\dot{T}_{3\text{solid}} = u_{\text{exog}} - k_{T3\text{dissolv}}T_{3\text{solid}} \quad \text{See Methods}$$

$$\dot{T}_{3\text{dissolv}} = k_{T3\text{dissolv}}T_{3\text{solid}} - (k_{T3\text{absorp}} + k_{T3\text{deg}})T_{3\text{dissolv}} \quad \text{See Methods}$$

$$\dot{T}_{4SC} = u_{\text{exog}} - k_{SC}T_{4SC} \quad \text{See Methods}$$

$$\dot{T}_{4IM} = u_{\text{exog}} - k_{IM}T_{4IM} \quad \text{See Methods}$$

Original TH Submodel Parameter Values [Details Given in Table 1 of Ref. (1)].

$A = 0.000289$; $B = 0.000214 \mu\text{mol}^{-1}$; $C = 0.000128 \mu\text{mol}^{-2}$; $D = -8.83 \times 10^{-6} \mu\text{mol}^{-3}$;
 $a = 0.00395$; $b = 0.00185 \mu\text{mol}^{-1}$; $c = 0.000610 \mu\text{mol}^{-2}$; $d = 0.000505 \mu\text{mol}^{-3}$;
 $k_{02} = 0.0189 \text{ h}^{-1}$; $k_{05} = 0.207 \text{ h}^{-1}$; $k_{12} = 0.868 \text{ h}^{-1}$; $k_{13} = 0.108 \text{ h}^{-1}$; $k_{45} = 5.37 \text{ h}^{-1}$;
 $k_{46} = 0.0689 \text{ h}^{-1}$; $k_{21\text{free}} = 1503 \text{ h}^{-1}$; $k_{31\text{free}} = 584 \text{ h}^{-1}$; $k_{54\text{free}} = 2043 \text{ h}^{-1}$; $k_{64\text{free}} = 127 \text{ h}^{-1}$;
 $k_{21} = 0.544 \text{ h}^{-1}$; $k_{31} = 0.211 \text{ h}^{-1}$; $k_{54} = 9.24 \text{ h}^{-1}$; $k_{64} = 0.573 \text{ h}^{-1}$

